Selective photocatalytic CO_2 reduction in water through anchoring of a molecular Ni catalyst on CdS nanocrystals

Moritz F. Kuehnel,[‡] Katherine L. Orchard,[‡] Kristian E. Dalle and Erwin Reisner*

Christian Doppler Laboratory for Sustainable SynGas Chemistry, Department of Chemistry, University of Cambridge, Lensfield Road, CB2 1EW, Cambridge, UK.

*Corresponding author email address: reisner@ch.cam.ac.uk

ABSTRACT: Photocatalytic conversion of CO_2 into carbonaceous feedstock chemicals is a promising strategy to mitigate greenhouse gas emissions and simultaneously store solar energy in chemical form. Photocatalysts for this transformation are typically based on precious metals and operate in non-aqueous solvents to suppress competing H_2 generation. In this work, we demonstrate the first example of selective visible-light driven CO_2 reduction in water using a synthetic photocatalyst system that is entirely free of precious metals. We present a series of self-assembled nickel terpyridine complexes as electrocatalysts for the reduction of CO_2 to CO in organic media. Immobilization on CdS quantum dots allows these catalysts to be active in purely aqueous solution and photocatalytically reduce CO_2 with >90% selectivity under UV-filtered simulated solar light irradiation (AM 1.5G, 100 mW cm^{-2}, $\lambda > 400$ nm, pH 6.7). Correlation between catalyst immobilization efficiency and product selectivity shows that anchoring the molecular catalyst on the semiconductor surface is key in controlling the selectivity for CO_2 reduction over H_2 evolution in aqueous phase.

INTRODUCTION

Overcoming the global dependence on fossil fuels is a central challenge of the 21st century,[1] and harvesting solar energy to convert water and carbon dioxide into feedstock chemicals is a promising strategy to utilize CO_2 and simultaneously store solar energy in chemical form.[2] For such an artificial photosynthesis approach to be widely applicable, the employed photocatalyst system should be based on inexpensive and earth-abundant materials and operate in aqueous solution, which allows the electrons required for CO_2 reduction to be sourced from water oxidation.[3] However, aqueous CO_2 reduction is challenging since CO_2 has a low solubility in water and the presence of excess protons promotes the competing H_2 evolution reaction, which is kinetically and thermodynamically more favorable than CO_2 reduction to CO.[4]

Particle-based photocatalysts have been widely studied for H_2 production and remain an important area of study since suspension-based reactors have been predicted to be cost-competitive for future widespread solar fuel production.[5] Such systems are typically multi-component, coupling photoactive particles with efficient electrocatalysts to form hybrid photocatalysts. For CO_2 reduction in particular, enhanced product selectivity can be achieved by employing highly selective molecular complexes as the electrocatalyst.[6] Semiconductor quantum dots (QDs) are attractive photosensitizers since they feature high extinction coefficients for visible light and long-lived excited states, compatible with the timescales of substrate turnover at the catalyst.[7] Covalent immobilization of catalysts onto the nanoparticle surface can further improve performance by enhancing charge-transfer rates between the photosensitizer and the catalyst compared to the non-immobilized case.[8]

A number of hybrid photocatalysts[9,10,11,12] and photoelectrodes[13,14] based on precious metal catalysts have been studied for CO_2 reduction, mostly in organic solvents. Recent work by Ishitani and co-workers has shown that selective photocatalytic CO_2 reduction to formic acid can be achieved in aqueous solution by interfacing highly active molecular Ru complexes with Ag/TaON[15] or Ag/C_3N_4[16] light absorbers. Fully precious-metal free synthetic photocatalyst systems are only known in organic solvent.[17,18] Selective photochemical CO_2 reduction to CO in aqueous solution without precious metals has been achieved with a bio-hybrid system based on CdS nanoparticles modified with a carbon monoxide dehydrogenase (CODH).[19] However, CODH is an extremely air-sensitive and fragile enzyme that is also expensive to isolate and purify and a maximum quantum yield of only 0.01% was achieved with this photocatalytic system.

In this work, we aimed to develop a hybrid photocatalyst system for CO_2 reduction in water that shows a high performance without containing precious metals either in the catalyst or the dye. A number of earth-abundant molecular electrocatalysts have been developed with good activity for CO_2 reduction in organic media[20] and in aqueous solution.[21] However, successful integration of these catalysts into a photocatalytic system has rarely been achieved in water since the overpotentials required to drive efficient CO_2 reduction with these catalysts are often too negative to be driven by common semiconductors and favor generation of substantial amounts of H_2. Photochemical CO_2 reduction in water has been reported using inexpensive Ni(cyclam) catalysts with Ru-based dyes,[8b,22] reaching a maximum TON per catalyst of 4.8 and a CO vs. H_2 generation selectivity of 20%.[8b]

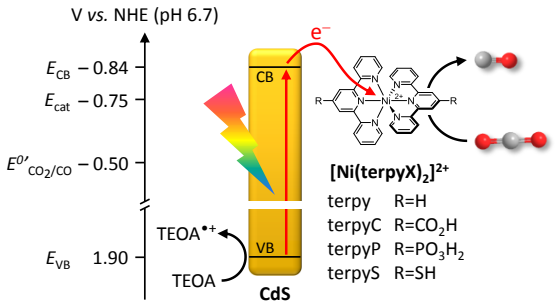

Figure 1. Schematic representation of the hybrid photocatalyst system developed in this work: A molecular nickel bis(terpyridine) catalyst anchored on a CdS quantum dot photosensitizer; different anchoring groups were studied for their performance.

Metal polypyridine complexes have been widely studied as electrocatalysts for CO_2 reduction,[23] but derivatives containing first row transition metals have been much less explored.[12b,17a-c,20e,24] Iron, cobalt, and nickel complexes with 2,2':6',2"-terpyridine (terpy) were first discovered to exhibit CO_2 reduction activity in the 1990s,[24a] and were recently revisited in more detail by Fontecave et al.[24b] $[Ni(terpy)_2]^{2+}$ showed a high selectivity for electrocatalytic CO generation in organic solvents at a low overpotential and a high selectivity for CO_2 reduction over H_2 generation, making it an attractive candidate for photocatalytic systems.[24b] CO is among the most versatile CO_2 reduction products because of its ease of separation from the reaction and its potential application for the synthesis of liquid fuels via Fischer-Tropsch chemistry.[25] The ease of modification of the terpy ligand (a range of derivatives are commercially available) also makes $[Ni(terpy)_2]^{2+}$ a versatile target for immobilization onto nanoparticulate photosensitizers. However, light-driven CO_2 reduction with 3d metal polypyridine complex has not been reported in water and without precious metal photosensitizers.

Here, we show that $[Ni(terpy)_2]^{2+}$ complexes are water-tolerant in electrochemical CO_2 reduction and that, by anchoring these complexes onto CdS QDs (Figure 1) their catalytic activity can be preserved in purely aqueous solution. The thus-formed hybrid photocatalyst operates with high selectivity (>90%) for CO_2 reduction under visible light irradiation, representing the first fully non-precious metal synthetic photocatalyst system for selective CO_2 reduction in water.

EXPERIMENTAL SECTION

Materials. All chemicals were obtained from commercial sources in the highest available purities and used as received. $Ni(BF_4)_2\times 6H_2O$ (99%) was purchased from Acros Organics, and 2,2':6',2"-terpyridine (terpy, 97%) was purchased from Alfa Aesar. 2,2':6',2"-terpyridine-4'-carboxylic acid (terpyC, 98%), 2,2':6',2"-terpyridine-4'-phosphonic acid (terpyP, 98%) and 2,2':6',2"-terpyridine-4'-thiol (terpyS, 98%) were purchased form HetCat, Switzerland. $Zn(BF_4)_2\times H_2O$ (18% Zn min) was purchased from Alfa Aesar. Ligand-free CdS QDs (QD-BF_4) were prepared according to a literature procedure (see Supporting Information for details).[26]

Assembly of catalysts, $[Ni(terpyX)_2]^{2+}$. An acetonitrile solution of $Ni(BF_4)_2\times 6H_2O$ (500 µL, 20 mM) was added to a glass vial containing terpyX (20 µmol). The mixture was diluted to 1 mL with acetonitrile (500 µL; terpy, terpyS) or water (terpyC, terpyP) and sonicated for 10 min to give a clear yellow-orange stock solution (See Figures S1, S3-S5 for characterization). Analogous $[Zn(terpyX)_2]^{2+}$ complexes were assembled in a similar fashion, using $Zn(BF_4)_2\times H_2O$.

Electrochemical procedures. Cyclic voltammetry (CV) was performed at room temperature under an atmosphere of Ar or CO_2 using a PalmSens EmStat potentiostat. A standard three-electrode cell was used for all measurements with a platinum mesh counter and a Ag/AgCl reference electrode (BASi), separated from the bulk solution by a porous Vyvor® frit. In anhydrous DMF or ACN solution (0.1 M Bu_4NBF_4, electrochemistry grade, Sigma Aldrich), a glassy carbon disc (3 mm diameter, BASi) or polycrystalline boron-doped diamond (BDD, purchased from Element Six and prepared into 1 mm glass-sealed disc electrodes using the facilities at the Warwick Electrochemistry and Interfaces Group) was used as working electrode; in aqueous solution (0.1 M TEOA, 0.1 M KCl, pH 6.7), a BDD electrode was used. Working electrodes were cleaned before experiments by mechanically polishing in alumina (Buehler, Micropolish, 1 µm) on a polishing cloth (Buehler, Microcloth). CVs were recorded at 0.1 V s^{-1} scan rate and 1.0 mM analyte concentration unless otherwise stated, solvents were purged for 10 min with the chosen gas saturated with solvent vapor prior to measurements (pH was measured after purging). The Fc/Fc^+ couple was used as an internal reference in organic media. Where necessary, literature potentials were converted from the normal hydrogen electrode (NHE) or Ag/AgCl electrode using published values.[27]

Spectro-electrochemistry was performed in an optically transparent thin-layer electrochemical cell with Pt mesh working and counter electrodes and a Ag wire quasi reference electrode,[28] filled with a solution of $Ni(BF_4)_2\times 6H_2O$ (0.1 mM for UV-vis, 3.0 mM for IR), terpy (0.2 mM for UV-vis, 6.0 mM for IR), Bu_4NBF_4 (0.01 M for UV-vis, 0.3 M for IR) in dry MeCN purged with Ar or CO_2. The potential was stepped in 50 mV intervals, held for 120 s before UV-vis or FTIR spectra were collected.

Controlled-potential electrolysis (CPE) was performed on a PalmSens Multistat using three parallel electrochemical cells of known volume under a CO_2 (2% CH_4) atmosphere using a glassy carbon rod working electrode; the counter electrode was separated from the working electrode by a coarse glass frit. Gaseous reaction products were quantified by gas chromatography, formic acid and oxalic acid in solution were quantified by ion chromatography at the end of the experiment.

Photocatalytic CO_2 reduction. In a typical experiment, QD-BF_4 stock solution in DMF (135 µM, 14.8 µL) was added to a pyrex photoreactor (Chromacol 10-SV, Fisher Scientific) containing a magnetic stirrer bar and the DMF was removed in vacuo. The particles were suspended in an aqueous solution of triethanolamine (TEOA, 0.1 M, 1.98 mL) and a stock solution of the self-assembled electrocatalyst (10 mM in acetonitrile or acetonitrile/water 1:1, 20 µL) was added. The photoreactor was sealed with a rubber septum and purged with CO_2 (containing 2% CH_4 as internal standard) for 10 min in the dark; the solution pH decreased from 10.1 to 6.7 after purging due to saturation with CO_2. The photoreactor was then placed in a water bath maintained at 25°C, stirred and irradiated by a solar light simulator (Newport Oriel, 100 mW cm^{-2}) equipped with an air mass 1.5 global filter (AM1.5G). IR irradiation was filtered with a water filter (10 cm path length) and UV irradiation with a 400 nm cut-off filter (UQG Optics) unless other-

wise stated. Product distribution was quantified through periodic headspace gas analysis (50 µL) by gas chromatography. Formic acid and oxalic acid in solution were quantified by ion chromatography at the end of the experiment.

Isotopic labeling. Photocatalysis experiments were performed as described above, but using $^{13}CO_2$ as the headspace gas. After 8 h, the photoreactor headspace was transferred to an evacuated gas IR cell (SpecAc, 10 cm path length, equipped with KBr windows) and a high-resolution transmission spectrum was collected.

RESULTS AND DISCUSSION

Electrochemical Characterization

Synthesis of the $[Ni(terpy)_2]^{2+}$ complexes was achieved by a simple self-assembly procedure, which allowed screening of electrochemical properties without time-consuming isolation of the complexes.[29] Cyclic voltammetry (CV) of the complex formed by self-assembly of $Ni(BF_4)_2{\times}6H_2O$ with 2 equivalents of terpy showed comparable redox features to those of the isolated $[Ni(terpy)_2]^{2+}$ complex[24b] (1 mM Ni^{2+}, 0.1 M Bu_4NBF_4 in Ar or CO_2-saturated DMF, Figure 2A). Monitoring the growth of the characteristic reduction waves of $[Ni(terpy)_2]^{2+}$ upon successive addition of terpy equivalents to a $Ni(BF_4)_2{\times}6H_2O$ solution indicates that the self-assembly process is rapid (Figure 2B). The catalyst identity was further corroborated by mass spectrometry and UV-vis spectroscopy (Figure S1).

CV of $[Ni(terpy)_2]^{2+}$ shows two reversible reduction waves at $E_{1/2}$ = –1.58 V and –1.76 V vs. Fc/Fc^+ (Figure S1B), with the first reduction showing considerable current enhancement under CO_2. Comparison with the corresponding $[Zn(terpy)_2]^{2+}$ complex (Figure S2A) confirms both reductions to be ligand-based, in agreement with previous literature assignments.[24b,30] UV-visible spectro-electrochemical measurements of $[Ni(terpy)_2]^{2+}$ (**a**) under Ar show the disappearance of the peak at 320 nm upon the first reduction followed by growing in of the peak at 235 nm upon further reduction (Figure 3A). Under CO_2, the second reduced species (at 235 nm) is no longer visible (Figure 3B), suggesting the first reduced species (**b**, Figure 3D) reacts with CO_2.

This was confirmed by FTIR spectro-electrochemistry under CO_2 (Figure 3C), which showed two bands at 1684 and 1642 cm^{-1} consistent with formation of a Ni-CO_2^- or Ni-CO_2H complex (**c** or **d**, Figure 3D).[31] Two additional peaks were detected at 1978 and 1899 cm^{-1} (Figure 3C), which we assign to carbonyl stretches of a Ni-CO complex (**e**, Figure 3D). In accordance with previous reports,[24b] we propose a reaction mechanism (Figure 3D, 3E) in which the singly reduced $[Ni(terpy)_2]^+$-complex (**b**) loses a terpy ligand upon reaction with CO_2 to give the Ni-CO_2 complex (**c**). A second ligand-based reduction to (**d**) is followed by reaction with CO_2 to give the Ni-CO complex (**e**). Since the electrocatalytic performance of $[Ni(terpy)_2]^{2+}$ is solvent-dependent (see below), we propose that vacant sites on the catalytically active Ni species are coordinated by solvent molecules.

With the catalytic activity of $[Ni(terpy)_2]^{2+}$ established, anchoring group-functionalized complexes $[Ni(terpyX)_2]^{2+}$ (X = C, P, S; Figure 1) were self-assembled using 2,2':6',2"-terpyridine-4'-phosphonic acid (terpyP), 2,2':6',2"-terpyridine-4'-thiol (terpyS), and 2,2':6',2"-terpyridine-4'-carboxylic acid (terpyC, see Figures S3-S5 for full characterization). The electrochemistry of the complexes was studied in 3:1 CH_3CN:H_2O solution to investigate their water tolerance. CV of $[Ni(terpyP)_2]^{2+}$ shows an electrochemical response comparable to the parent $[Ni(terpy)_2]^{2+}$ complex but shifted to more positive potentials (Figure S3B) as expected from substitution with an electron-withdrawing phosphonic acid group. The first cathodic wave is irreversible, indicative of structural rearrangements upon reduction. Comparison with the analogous $[Zn(terpyP)_2]^{2+}$ complex was not possible due to its low solubility in this solvent system.

$[Ni(terpyC)_2]^{2+}$ undergoes two irreversible reductions which are more anodically shifted then in $Ni(terpyP)_2]^{2+}$, presumably due to the strong electron-withdrawing nature of the carboxyl functionality on the ligand. A third, partly reversible reduction wave is observed at approximately –1.7 V (Figure S4B), which is also displayed by the analogous $[Zn(terpyC)_2]^{2+}$ complex and can therefore be assigned to another ligand based reduction (Figure S2B). CV of $[Ni(terpyS)_2]^{2+}$ shows a number of poorly resolved irreversible redox events (Figure S5B), which are similarly observed with $[Zn(terpyS)_2]^{2+}$. This again suggests ligand-based reductions (Figure S2C). CV of $[Ni(terpyS)_2]^{2+}$ is further complicated by the low solubility of the reduced complex, as indicated by a decrease in electrochemical response upon repeated cycling.

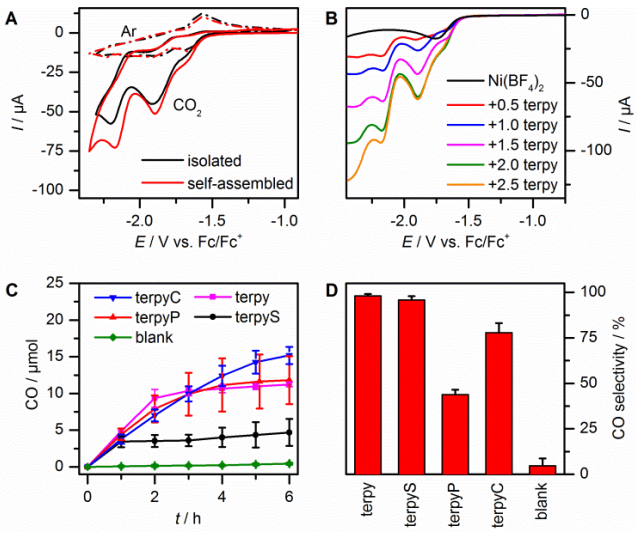

Figure 2. Self-assembled $[Ni(terpy)_2]^{2+}$ as selective electrocatalyst for CO_2 reduction. (A) Comparison of self-assembled vs. isolated complex under Ar and CO_2 (1.0 mM complex, 0.1 M Bu_4NBF_4 in DMF, 100 mV s^{-1}, rt); (B) Self-assembly of $[Ni(terpy)_2]^{2+}$ by consecutive addition of terpy ligand to $Ni(BF_4)_2{\times}6H_2O$ under a CO_2 atmosphere followed by linear sweep voltammetry (1.0 mM $Ni(BF_4)_2{\times}6H_2O$, 0.1 M Bu_4NBF_4 in DMF, 100 mV s^{-1}); (C) Electrocatalytic CO formation during CPE in the presence of self-assembled $[Ni(terpyX)_2]^{2+}$; (D) CO *vs.* H_2 electrolysis product selectivity after 1 h CPE. CPE conditions: E_{appl} = –1.83 V vs. Fc/Fc^+, 0.25 mM $[Ni(terpyX)_2]^{2+}$, 0.1 M Bu_4NBF_4 in acetonitrile/water 3:1 under CO_2, glassy carbon working, Ag/AgCl reference and Pt mesh counter electrodes, rt; X=C: CO_2H, P: PO_3H_2, S: SH (see Figure 1).

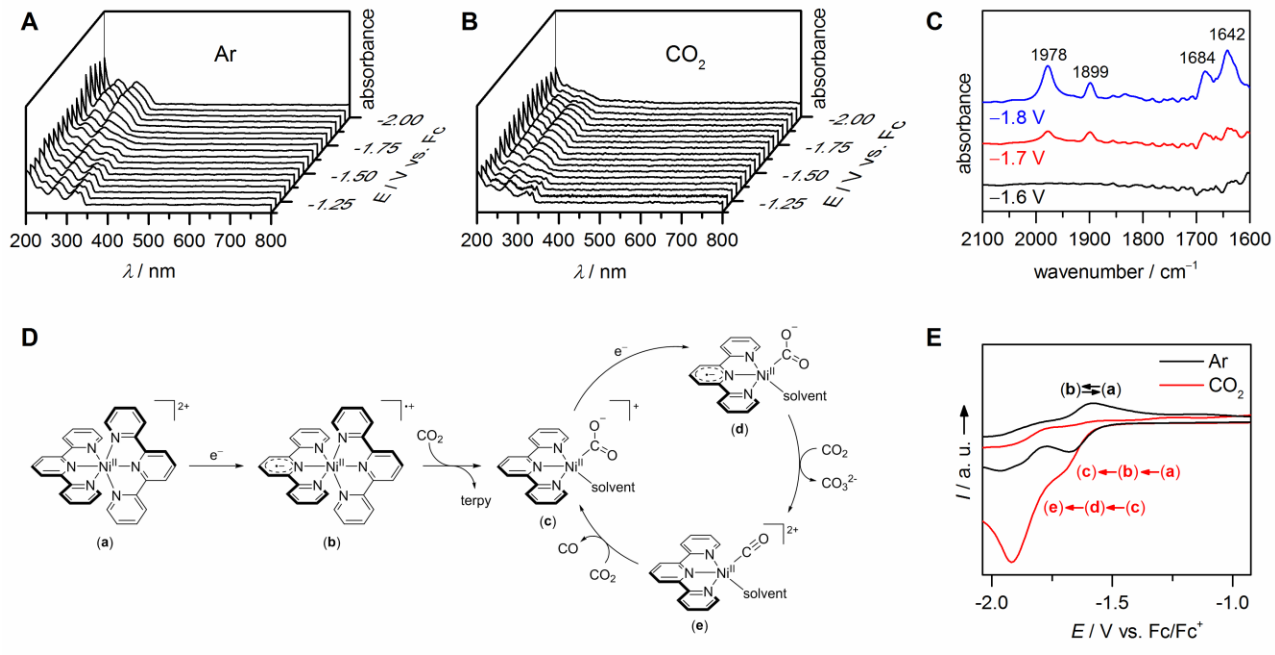

Figure 3. Mechanism of electrocatalytic CO_2 reduction with $[Ni(terpy)_2]^{2+}$. (A, B) UV-visible spectro-electrochemistry under Ar (A) and CO_2 (B) atmosphere; (C) FTIR spectro-electrochemistry under CO_2; (D) proposed mechanism of electrocatalytic CO_2 reduction; (E) cyclic voltammogram of $[Ni(terpy)_2]^{2+}$ with indicated reaction steps under Ar and CO_2. All experiments were performed in dry acetonitrile electrolyte solution.

Under CO_2, $[Ni(terpyC)_2]^{2+}$, $[Ni(terpyP)_2]^{2+}$ and $[Ni(terpyS)_2]^{2+}$ all exhibit modest current enhancements, indicative of electrocatalytic activity towards CO_2. CO_2 reduction was confirmed by controlled-potential electrolysis (CPE, E_{appl} = –1.83 V vs. Fc/Fc^+; Figure 2C). In line with previous reports,[24b] CO was detected as the sole CO_2 reduction product with all catalysts, as formation of formic acid and oxalate was excluded using ion chromatography. The selectivity for CO_2 reduction over proton reduction varied with the employed ligand, with over 95% selectivity being achieved in the first hour for both $[Ni(terpy)_2]^{2+}$ and $[Ni(terpyS)_2]^{2+}$ (Figure 2D). Up to 8.5 turnovers (with respect to Ni) were achieved over 12 h CPE with $[Ni(terpyC)_2]^{2+}$ and all catalysts significantly exceeded the performance of previous reports in dry DMF (TON 0.1;† Table S1).[24b] We ascribe this difference in performance to variation of the solvent, as electrolysis in DMF and DMF/H_2O mixtures gave a much lower catalytic activity. This finding is consistent with a solvent-coordinated catalytically active species (Figure 3D).

The electrochemical behavior of the $[Ni(terpyX)_2]^{2+}$ complexes was further investigated in purely aqueous solution to evaluate their potential use in hybrid photocatalysis in the absence of organic solvents. The electrochemical response in water was markedly different from that in organic media (Figures S1D, S3D, S4D, S5D). All observed redox events were irreversible presumably due to structural changes during reduction, e.g. loss of a ligand, which is insoluble in water. In addition, $[Ni(terpy)_2]^{2+}$ and $[Ni(terpyP)_2]^{2+}$ showed anodic stripping peaks on the return scan, suggesting a low solubility of the reduced species and/or catalyst decomposition. Under CO_2, $[Ni(terpyC)_2]^{2+}$ and $[Ni(terpyS)_2]^{2+}$ both showed a current enhancements indicative of electrocatalytic activity for CO_2 reduction (E_{onset} = –0.85 V and –0.75 V vs. NHE, respectively), whereas $[Ni(terpy)_2]^{2+}$ and $[Ni(terpyP)_2]^{2+}$ showed changes in their electrochemical response, indicative of reactivity towards CO_2 but with no clear catalytic wave. Electrocatalytic activity of $[Ni(terpyX)_2]^{2+}$ towards CO_2 was confirmed by performing CPE in aqueous solution under CO_2 (E_{appl} = –0.84 V vs. NHE, 0.5 mM catalyst, 0.1 M $KHCO_3$, pH 6.7). Formation of small amounts of CO was observed with all complexes (Table S2), but the catalytic activity decayed rapidly, accompanied by the formation of a deposit on the working electrode.

Photocatalytic CO_2 Reduction

The hybrid photocatalyst system was assembled by combining the $[Ni(terpyX)_2]^{2+}$ catalysts with CdS quantum dots (QDs, D = 5.3 nm, λ_{max} = 451 nm, Figure S6A). CdS is an inexpensive semiconductor with a tunable visible light absorption. Previous work in our laboratory has shown that ligand-free, charge-stabilized CdS QDs (QD-BF_4) show excellent photocatalytic activity for H_2 evolution in pH-neutral aqueous solution.[26,32] CV of CdS-BF_4 immobilized on a glassy carbon electrode were used to electrochemically determine[33] the conduction band (CB) edge potential in aqueous solution (0.1 M triethanolamine, TEOA, pH 6.7; Figure S6B). A measured value of E_{CB} = –0.84 V vs. NHE suggests enough driving force to enable efficient CO_2 reduction at $[Ni(terpyS)_2]^{2+}$, which shows an onset of catalysis at –0.75 V vs. NHE under the same conditions.

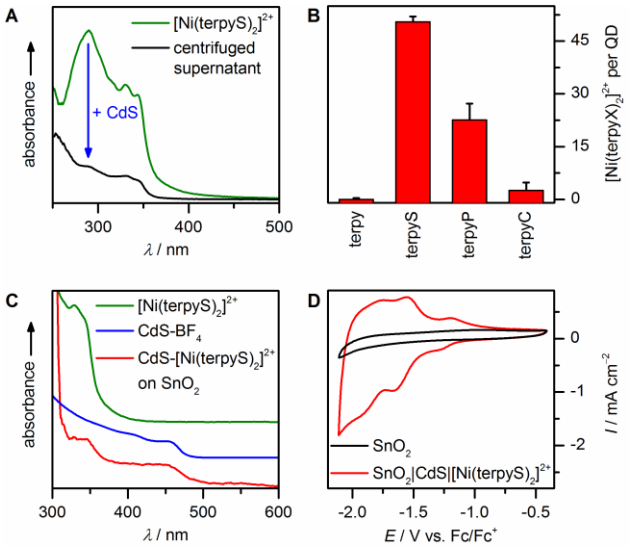

Figure 4. Hybrid photocatalyst assembly from CdS QDs and $[Ni(terpyX)_2]^{2+}$. A) Difference in UV-vis absorption of a $[Ni(terpyS)_2]^{2+}$ solution (100 µM, 0.1 M aq. TEOA, pH 6.7) before and after stirring with CdS QDs (1 µM QD-BF_4); B) Adsorption efficiency of different $[Ni(terpyX)_2]^{2+}$ complexes (addition of 1 µM QD-BF4 to 100 µM $[Ni(terpyX)_2]^{2+}$ in 0.1 M aq. TEOA, pH 6.7); C) UV-vis spectra of CdS-$[Ni(terpyS)_2]^{2+}$ hybrid photocatalyst immobilized on a mesoporous SnO_2 electrode and comparison with CdS-BF_4 and $[Ni(terpyS)_2]^{2+}$ in solution (spectra scaled and stacked for clarity); D) Cyclic voltammetry of CdS-$[Ni(terpyS)_2]^{2+}$ photocatalyst immobilized on a SnO_2 electrode (0.1 M Bu_4NBF_4 in acetonitrile under Ar, Ag/AgCl reference and Pt mesh counter electrodes, rt).

Modification of QD-BF_4 was carried out in situ by adding a stock solution of a self-assembled Ni complex to a suspension of QDs in aqueous TEOA solution (0.1 M). The final solution composition of H_2O:CH_3CN was 99:1 for $[Ni(terpy)_2]^{2+}$and $[Ni(terpyS)_2]^{2+}$, and 99.5:1 for $[Ni(terpyC)_2]^{2+}$ and $[Ni(terpyP)_2]^{2+}$. Catalyst attachment was confirmed by UV-vis spectroscopy with the catalyst loading dependent on the anchoring group (Figure 4A). The highest loading (50.5±2.9 nmol cat. per nmol QD) was achieved with the thiol derivative, $[Ni(terpyS)_2]^{2+}$, with significantly lower affinity measured for the other anchors (Figure 4B). The appearance of characteristic catalyst peaks in the UV-vis and ATR-IR spectra of $[Ni(terpyS)_2]^{2+}$–modified CdS QDs immobilized on a mesoporous SnO_2 electrode confirmed that the catalyst remained structurally intact on the QD surface (Figures 4C and S7). CV showed that the anchored catalyst retained its electrochemical response, further corroborating functional integrity on the QD surface (Figure 4D). Transmission electron microscopy showed that anchoring of the catalyst does not affect the particle morphology or dispersibility (Figure S8).

The photocatalytic activity of the assembled CdS-$[Ni(terpyX)_2]^{2+}$ hybrids was assessed in CO_2-saturated water under simulated solar light irradiation in the presence of TEOA as a sacrificial electron donor (0.1 M, pH 6.7, 100 mW cm^{-2} AM1.5G, λ > 400 nm, 25°C; Table S3). Whereas the parent CdS-$[Ni(terpy)_2]^{2+}$ catalyst without an anchoring group generated mainly H_2 and only traces of CO, the functionalized derivatives showed considerably higher activities towards CO_2 reduction (Figure 5A, Table S3). $[Ni(terpyS)_2]^{2+}$ exhibited both the highest CO_2 reduction activity and product selectivity of this series (92.2% after 4 h compared to 10.2% and 3.9% for $[Ni(terpyP)_2]^{2+}$ and $[Ni(terpyC)_2]^{2+}$, respectively). Strikingly, the observed selectivity does not reflect the electrocatalytic activity in homogeneous phase (Figure 3C-D, Table S2), but correlates with the adsorption efficiency of each complex to CdS (Figure 5B). This trend confirms that interfacing the molecular catalyst with the nanoparticle is key to overall photocatalytic activity in aqueous solution. Since CdS QDs alone only produced trace amounts of CO and addition of a Ni salt only enhanced the production of H_2 (Figure S8, Table S3), it can be concluded that the active species for CO production is the molecular catalyst. X-ray photoelectron spectroscopy of CdS-$[Ni(terpyS)_2]^{2+}$ after 1 h irradiation was performed to characterize the Ni species present when the hybrid photocatalyst shows its peak performance (Figure S10). The observed Ni($2p_{3/2}$) binding energy of 856.6 eV is consistent with a molecular Ni^{II} species, ruling out potential formation of elemental Ni and NiS which would be expected at close to 853 eV.[34] CO_2 was unambiguously confirmed as the sole origin of the formed CO through gas-phase IR spectroscopy using $^{13}CO_2$ to give ^{13}CO exclusively (Figure S11). Other CO_2 reduction products such as formic acid and oxalate could not be detected in the reaction solution by ion chromatography. Photocatalysis experiments performed without a UV cut-off filter resulted in little difference in TON_{CO} compared to visible-light only, indicating that the catalytic reaction rate is limiting rather than light absorption (Table S3). Using acetonitrile/water mixtures as reaction medium analogous to those used in electrochemical analysis only led to a small increase in activity accompanied by a lower product selectivity (Figure S12, Table S3).

Under optimized conditions, up to 20 Ni-based turnovers were achieved with CdS-$[Ni(terpyS)_2]^{2+}$ during 24 h visible-light illumination (Figure 5C, Table S3). CO selectivity remains above 90% for the first 8 hours, before it gradually decreases to produce predominantly H_2 after 24 h. Ion-coupled plasma optical emission spectroscopy (ICP-OES) of QDs isolated from the reaction medium confirms that the decreasing selectivity coincides with a gradual loss of $[Ni(terpyS)_2]^{2+}$ from the QD surface (Figure 5D, Table S4), whereas the CdS-BF_4 particles remain intact. UV-vis spectra show a slight red-shift of the first excitonic absorption, indicative of limited particle aggregation without significant photocorrosion (Figure S13A). Addition of fresh catalyst after 20 h recovers the CO generation activity and suppresses H_2 evolution (Figure 5C), while adding $Ni(BF_4)_2$ only promotes H_2 evolution (Figure S14). Conversely, lowering the initial catalyst:QD ratio lowered the CO selectivity but did not significantly affect the maximum TON_{CO} (with respect to $[Ni(terpyS)_2]^{2+}$, Figure S15), from which it can be inferred that a TON_{CO} of ~20 represents a limit of stability of the catalyst.

Stirring CdS-$[Ni(terpyS)_2]^{2+}$ in the dark had no effect on the photocatalytic activity, therefore catalyst deactivation is dependent only on catalyst turnover (Figure S16). Release of a terpyS ligand during catalytic turnover was monitored by trapping the intact ligand with Fe^{2+} ions. UV-vis quantification of the formed $[Fe(terpyS)_2]^{2+}$ complex (based on the absorption at 578 nm; Figure S13B-D) showed that approximately 30% of the initial ligand loading was recovered. Loss of the remaining 70%, suggests that the ligand itself degrades during catalyst turnover (Figure S13D). It has been proposed that $[Ni(terpy)_2]^{2+}$ deactivates during catalysis due to *N*-carboxylation of the ligand.[24b,35]

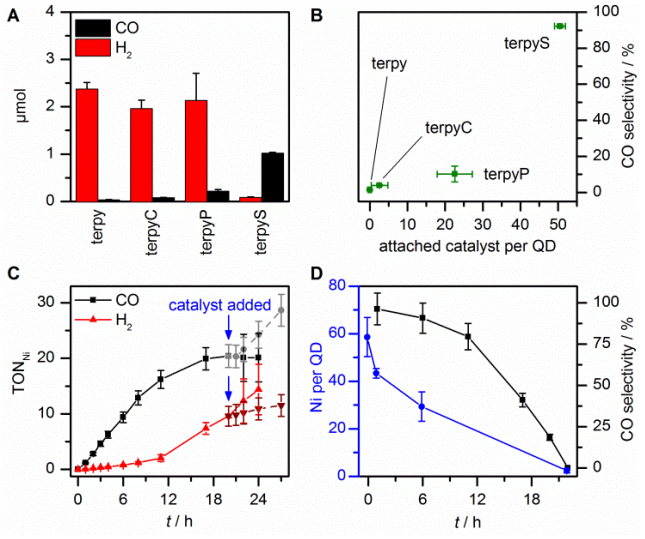

Figure 5. Photocatalytic reduction of aqueous CO_2 in the presence of CdS-$[Ni(terpyX)_2]^{2+}$ hybrid catalysts. A) Effect of different anchoring groups on the product selectivity (4 h irradiation; see Figure S9 for control experiments); B) Correlation of product selectivity with catalyst attachment (4 h irradiation); C) Long-term activity of CdS-$[Ni(terpyS)_2]^{2+}$ (solid lines) and effect of adding more catalyst after 20 h (dashed lines); D) Changes in product selectivity and catalyst loading over time for CdS-$[Ni(terpyS)_2]^{2+}$. Photocatalysis conditions: 100 mW cm^{-2}, AM1.5G, λ>400 nm, 1 µM QD, 100 µM $[Ni(terpyX)_2]^{2+}$, 25°C.

It is notable that the Ni loading of the CdS QDs after CO production ceases (24 h for initial loading of 100:1 Ni:QD) is comparable to that measured for systems that only produced H_2 (QDs with $[Ni(terpy)_2]^{2+}$ and $Ni(BF_4)_2$, Table S4). We conclude that highly selective CO production occurs by electron transfer from the QDs to the molecular catalyst while the catalyst remains attached to the surface. As the catalyst is lost from the QDs, H_2 production can occur at the exposed CdS surface, presumably promoted by Ni ions released upon decomposition of $[Ni(terpyS)_2]^{2+}$. Ni is a known co-catalyst for photocatalytic H_2 evolution from Cd-based QDs.[36] Control experiments with CdS-$[Ni(terpyX)_2]^{2+}$ in the absence of CO_2 further corroborated the role of the surface-functionalization in controlling H_2 evolution (Figure S17, Table S5). In the presence of the freely diffusing co-catalyst $[Ni(terpy)_2]^{2+}$, QD-BF_4 steadily evolved H_2 under illumination. In contrast, in the presence of $[Ni(terpyS)_2]^{2+}$ which binds strongly to the QD surface, H_2 evolution was significantly suppressed during the first 2 h. Under prolonged irradiation, the rate of H_2 generation from CdS-$[Ni(terpyS)_2]^{2+}$ increased and was comparable to that observed under CO_2. Co-catalyst re-addition after 17 h reduced H_2 evolution, further demonstrating that surface-attached $[Ni(terpyS)_2]^{2+}$ prevents H_2 formation, even in the presence of decomposition-derived Ni in solution. The use of mercaptopropionic acid-capped QDs (QD-MPA) to deliberately block the QD surface[32] did not result in higher selectivity, but lowered the overall activity (Figure S18, Table S3), presumably due to inhibited access of the catalyst to the surface.

For CdS-$[Ni(terpyS)_2]^{2+}$, the average external quantum efficiency (EQE) for CO production under 400 nm monochromatic light (1.5 mW cm^{-2}) was 0.28 ± 0.04% (highest 0.31%, average taken for linear activity between 4 and 8 h; Table S6). Comparable EQE was previously reported for CO_2 to formate conversion with a precious-metal containing Ru-Ag-TaON hybrid catalyst at similar pH (EQE_{HCOOH} = 0.23%, pH 7.0, 0.1 M Na_2CO_3).[15] In this system, higher efficiency was obtained at lower pH (EQE_{HCOOH} = 0.47%, pH 4.3, no Na_2CO_3) but bulk product selectivity was reduced (37% c.f. 85%).[15] Higher efficiencies have been achieved by homogeneous precious-metal based photocatalysts,[37] with a Ru-Re photocatalyst achieving 13% EQE and TON 130 in water (81% CO selectivity).[37a]

CONCLUSION

In summary, we have demonstrated that self-assembled nickel bis(terpyridine) complexes are tolerant to water in electrocatalytic reduction of CO_2 in organic solution. Anchoring these catalysts on CdS quantum dots transfers this activity into pure water to achieve visible-light driven reduction of aqueous CO_2. The performance of this hybrid system was found to crucially depend on the interface between the nanoparticulate photosensitizer and the molecular catalyst, demonstrating that catalyst immobilization is key to achieve selective CO_2 reduction in water. More than 90% selectivity for CO generation was achieved with the catalyst with the highest affinity for the QDs, $[Ni(terpyS)_2]^{2+}$. To the best of our knowledge, this is the first example of a precious-metal free synthetic photocatalyst system capable of selective CO_2 reduction in an aqueous medium under visible-light irradiation.

ASSOCIATED CONTENT

Supporting Information

Electronic Supplementary Information (ESI) available free of charge on the ACS Publications website: Experimental procedures, electrochemical and spectroscopic data (PDF).

AUTHOR INFORMATION

Corresponding Author

*reisner@ch.cam.ac.uk.

ORCID

Moritz F. Kuehnel: 0000-0001-8678-3779
Katherine Orchard: 0000-0002-6349-1316
Erwin Reisner: 0000-0002-7781-1616

Author Contributions

‡These authors contributed equally.

Notes

†TON was calculated by dividing the moles of formed CO (~2.5 µmol) by the moles of catalyst used (10 mL, 2 mM = 20 µmol $[Ni(terpy)_2]^{2+}$).

ACKNOWLEDGMENT

This work was supported by the Christian Doppler Research Association (Austrian Federal Ministry of Science, Research and Economy and the National Foundation for Research, Technology and Development), the OMV Group, the Isaac Newton Trust (12.38/k), the German Research Foundation (KU 3077/2-1 to MFK), and the World Premier International Research Center Initiative (WPI), MEXT, Japan (KLO). We thank Dr. David Wakerley, Ms. Christina Chang and Dr. Timothy Rosser for helpful discussions. We thank the Electrochemistry and Interfaces Group at The University of Warwick for kindly providing access to their facilities to assemble the BDD electrode.

REFERENCES

(1) Armaroli, N.; Balzani, V. *Angew. Chem., Int. Ed.* **2007**, *46*, 52-66.
(2) Olah, G. A.; Goeppert, A.; Prakash, G. K. S. *J. Org. Chem.* **2008**, *74*, 487-498.
(3) Kim, W.; Yuan, G.; McClure, B. A.; Frei, H. *J. Am. Chem. Soc.* **2014**, *136*, 11034-11042.
(4) (a) White, J. L.; Baruch, M. F.; Pander Iii, J. E.; Hu, Y.; Fortmeyer, I. C.; Park, J. E.; Zhang, T.; Liao, K.; Gu, J.; Yan, Y.; Shaw, T. W.; Abelev, E.; Bocarsly, A. B. *Chem. Rev.* **2015**, *115*, 12888-12935; (b) Costentin, C.; Robert, M.; Saveant, J.-M. *Chem. Soc. Rev.* **2013**, *42*, 2423-2436.
(5) (a) Fabian, D. M.; Hu, S.; Singh, N.; Houle, F. A.; Hisatomi, T.; Domen, K.; Osterloh, F. E.; Ardo, S. *Energy Environ. Sci.* **2015**, *8*, 2825-2850; (b) Pinaud, B. A.; Benck, J. D.; Seitz, L. C.; Forman, A. J.; Chen, Z.; Deutsch, T. G.; James, B. D.; Baum, K. N.; Baum, G. N.; Ardo, S.; Wang, H.; Miller, E.; Jaramillo, T. F. *Energy Environ. Sci.* **2013**, *6*, 1983-2002; (c) Wang, Q.; Hisatomi, T.; Jia, Q.; Tokudome, H.; Zhong, M.; Wang, C.; Pan, Z.; Takata, T.; Nakabayashi, M.; Shibata, N.; Li, Y.; Sharp, I. D.; Kudo, A.; Yamada, T.; Domen, K. *Nat. Mater.* **2016**, *15*, 611-615; (d) Willkomm, J.; Orchard, K. L.; Reynal, A.; Pastor, E.; Durrant, J. R.; Reisner, E. *Chem. Soc. Rev.* **2016**, *45*, 9-23.
(6) (a) Won, D.-I.; Lee, J.-S.; Ji, J.-M.; Jung, W.-J.; Son, H.-J.; Pac, C.; Kang, S. O. *J. Am. Chem. Soc.* **2015**, *137*, 13679-13690; (b) Li, K.; Peng, B.; Peng, T. *ACS Catal.* **2016**, *6*, 7485-7527; (c) Windle, C. D.; Reisner, E. *Chimia* **2015**, *69*, 435-441.
(7) Alivisatos, A. P. *J. Phys. Chem.* **1996**, *100*, 13226-13239.
(8) (a) Sato, S.; Morikawa, T.; Saeki, S.; Kajino, T.; Motohiro, T. *Angew. Chem., Int. Ed.* **2010**, *49*, 5101-5105; (b) Neri, G.; Forster, M.; Walsh, J. J.; Robertson, C.; Whittles, T.; Farras Costa, P.; Cowan, A. J. *Chem. Commun.* **2016**, *52*, 14200-14203.
(9) Muraoka, K.; Kumagai, H.; Eguchi, M.; Ishitani, O.; Maeda, K. *Chem. Commun.* **2016**, *52*, 7886-7889.
(10) (a) Maeda, K.; Kuriki, R.; Ishitani, O. *Chem. Lett.* **2016**, *45*, 182-184; (b) Kuriki, R.; Ishitani, O.; Maeda, K. *ACS Appl. Mater. Interfaces* **2016**, *8*, 6011-6018; (c) Kuriki, R.; Sekizawa, K.; Ishitani, O.; Maeda, K. *Angew. Chem., Int. Ed.* **2015**, *54*, 2406-2409; (d) Maeda, K.; Kuriki, R.; Zhang, M.; Wang, X.; Ishitani, O. *J. Mater. Chem. A* **2014**, *2*, 15146-15151; (e) Maeda, K.; Sekizawa, K.; Ishitani, O. *Chem. Commun.* **2013**, *49*, 10127-10129.
(11) (a) Windle, C. D.; Pastor, E.; Reynal, A.; Whitwood, A. C.; Vaynzof, Y.; Durrant, J. R.; Perutz, R. N.; Reisner, E. *Chem.--Eur. J.* **2015**, *21*, 3746-3754; (b) Ha, E.-G.; Chang, J.-A.; Byun, S.-M.; Pac, C.; Jang, D.-M.; Park, J.; Kang, S. O. *Chem. Commun.* **2014**, *50*, 4462-4464.
(12) (a) Lee, Y.; Kim, S.; Kang, J. K.; Cohen, S. M. *Chem. Commun.* **2015**, *51*, 5735-5738; (b) Fei, H.; Sampson, M. D.; Lee, Y.; Kubiak, C. P.; Cohen, S. M. *Inorg. Chem.* **2015**, *54*, 6821-6828; (c) Wang, S.; Yao, W.; Lin, J.; Ding, Z.; Wang, X. *Angew. Chem., Int. Ed.* **2014**, *53*, 1034-1038; (d) Wang, S.; Lin, J.; Wang, X. *Phys. Chem. Chem. Phys.* **2014**, *16*, 14656-14660.
(13) (a) Schreier, M.; Luo, J.; Gao, P.; Moehl, T.; Mayer, M. T.; Grätzel, M. *J. Am. Chem. Soc.* **2016**, *138*, 1938-1946; (b) Sahara, G.; Abe, R.; Higashi, M.; Morikawa, T.; Maeda, K.; Ueda, Y.; Ishitani, O. *Chem. Commun.* **2015**, *51*, 10722-10725; (c) Kou, Y.; Nakatani, S.; Sunagawa, G.; Tachikawa, Y.; Masui, D.; Shimada, T.; Takagi, S.; Tryk, D. A.; Nabetani, Y.; Tachibana, H.; Inoue, H. *J. Catal.* **2014**, *310*, 57-66.
(14) (a) Arai, T.; Sato, S.; Morikawa, T. *Energy Environ. Sci.* **2015**, *8*, 1998-2002; (b) Arai, T.; Sato, S.; Kajino, T.; Morikawa, T. *Energy Environ. Sci.* **2013**, *6*, 1274-1282; (c) Sato, S.; Arai, T.; Morikawa, T.; Uemura, K.; Suzuki, T. M.; Tanaka, H.; Kajino, T. *J. Am. Chem. Soc.* **2011**, *133*, 15240-15243; (d) Arai, T.; Sato, S.; Uemura, K.; Morikawa, T.; Kajino, T.; Motohiro, T. *Chem. Commun.* **2010**, *46*, 6944-6946.
(15) Nakada, A.; Nakashima, T.; Sekizawa, K.; Maeda, K.; Ishitani, O. *Chem. Sci.* **2016**, *7*, 4364-4371.
(16) Kuriki, R.; Matsunaga, H.; Nakashima, T.; Wada, K.; Yamakata, A.; Ishitani, O.; Maeda, K. *J. Am. Chem. Soc.* **2016**, *138*, 5159-5170.
(17) (a) Walsh, J. J.; Jiang, C.; Tang, J.; Cowan, A. J. *Phys. Chem. Chem. Phys.* **2016**, *18*, 24825-24829; (b) Takeda, H.; Ohashi, K.; Sekine, A.; Ishitani, O. *J. Am. Chem. Soc.* **2016**, *138*, 4354-4357; (c) Guo, Z.; Cheng, S.; Cometto, C.; Anxolabéhère-Mallart, E.; Ng, S.-M.; Ko, C.-C.; Liu, G.; Chen, L.; Robert, M.; Lau, T.-C. *J. Am. Chem. Soc.* **2016**, *138*, 9413-9416; (d) Lin, J.; Pan, Z.; Wang, X. *ACS Sustainable Chem. Eng.* **2014**, *2*, 353-358; (e) Jin, T.; Liu, C.; Li, G. *Chem. Commun.* **2014**, *50*, 6221-6224.
(18) (a) Rosser, T. E.; Windle, C. D.; Reisner, E. *Angew. Chem., Int. Ed.* **2016**, *55*, 7388-7392; (b) Torralba-Peñalver, E.; Luo, Y.; Compain, J.-D.; Chardon-Noblat, S.; Fabre, B. *ACS Catal.* **2015**, *5*, 6138-6147.
(19) Chaudhary, Y. S.; Woolerton, T. W.; Allen, C. S.; Warner, J. H.; Pierce, E.; Ragsdale, S. W.; Armstrong, F. A. *Chem. Commun.* **2012**, *48*, 58-60.
(20) (a) Rosas-Hernandez, A.; Alsabeh, P. G.; Barsch, E.; Junge, H.; Ludwig, R.; Beller, M. *Chem. Commun.* **2016**, *52*, 8393-8396; (b) Chapovetsky, A.; Do, T. H.; Haiges, R.; Takase, M. K.; Marinescu, S. C. *J. Am. Chem. Soc.* **2016**, *138*, 5765-5768; (c) Azcarate, I.; Costentin, C.; Robert, M.; Savéant, J.-M. *J. Am. Chem. Soc.* **2016**, *138*, 16639–16644; (d) Chen, L.; Guo, Z.; Wei, X.-G.; Gallenkamp, C.; Bonin, J.; Anxolabéhère-Mallart, E.; Lau, K.-C.; Lau, T.-C.; Robert, M. *J. Am. Chem. Soc.* **2015**, *137*, 10918-10921; (e) Chan, S. L.-F.; Lam, T. L.; Yang, C.; Yan, S.-C.; Cheng, N. M. *Chem. Commun.* **2015**, *51*, 7799-7801; (f) Lacy, D. C.; McCrory, C. C. L.; Peters, J. C. *Inorg. Chem.* **2014**, *53*, 4980-4988; (g) Clark, M. L.; Grice, K. A.; Moore, C. E.; Rheingold, A. L.; Kubiak, C. P. *Chem. Sci.* **2014**, *5*, 1894-1900; (h) Thoi, V. S.; Kornienko, N.; Margarit, C. G.; Yang, P.; Chang, C. J. *J. Am. Chem. Soc.* **2013**, *135*, 14413-14424; (i) Costentin, C.; Drouet, S.; Robert, M.; Savéant, J.-M. *Science* **2012**, *338*, 90-94; (j) Rail, M. D.; Berben, L. A. *J. Am. Chem. Soc.* **2011**, *133*, 18577-18579; (k) Bourrez, M.; Molton, F.; Chardon-Noblat, S.; Deronzier, A. *Angew. Chem., Int. Ed.* **2011**, *50*, 9903-9906.
(21) (a) Weng, Z.; Jiang, J.; Wu, Y.; Wu, Z.; Guo, X.; Materna, K. L.; Liu, W.; Batista, V. S.; Brudvig, G. W.; Wang, H. *J. Am. Chem. Soc.* **2016**, *138*, 8076-8079; (b) Tatin, A.; Comminges, C.; Kokoh, B.; Costentin, C.; Robert, M.; Savéant, J.-M. *Proc. Natl. Acad. Sci. U. S. A.* **2016**, *113*, 5526-5529; (c) Neri, G.; Aldous, I. M.; Walsh, J. J.; Hardwick, L. J.; Cowan, A. J. *Chem. Sci.* **2016**, *7*, 1521-1526; (d) Taheri, A.; Thompson, E. J.; Fettinger, J. C.; Berben, L. A. *ACS Catal.* **2015**, *5*, 7140-7151; (e) Shen, J.; Kortlever, R.; Kas, R.; Birdja, Y. Y.; Diaz-Morales, O.; Kwon, Y.; Ledezma-Yanez, I.; Schouten, K. J. P.; Mul, G.; Koper, M. T. M. *Nat. Commun.* **2015**, *6*, 8177; (f) Costentin, C.; Robert, M.; Savéant, J.-M.; Tatin, A. *Proc. Natl. Acad. Sci. U. S. A.* **2015**, *112*, 6882-6886; (g) Froehlich, J. D.; Kubiak, C. P. *Inorg. Chem.* **2012**, *51*, 3932-3934; (h) Beley, M.; Collin, J.-P.; Ruppert, R.; Sauvage, J.-P. *J. Chem. Soc., Chem. Commun.* **1984**, 1315-1316.
(22) (a) Mochizuki, K.; Manaka, S.; Takeda, I.; Kondo, T. *Inorg. Chem.* **1996**, *35*, 5132-5136; (b) Craig, C. A.; Spreer, L. O.; Otvos, J. W.; Calvin, M. *J. Phys. Chem.* **1990**, *94*, 7957-7960; (c) Grant, J. L.; Goswami, K.; Spreer, L. O.; Otvos, J. W.; Calvin, M. *J. Chem. Soc., Dalton Trans.* **1987**, 2105-2109.
(23) (a) Qiao, J.; Liu, Y.; Hong, F.; Zhang, J. *Chem. Soc. Rev.* **2014**, *43*, 631-675; (b) Savéant, J.-M. *Chem. Rev.* **2008**, *108*, 2348-2378.
(24) (a) Arana, C.; Yan, S.; Keshavarz-K, M.; Potts, K. T.; Abruna, H. D. *Inorg. Chem.* **1992**, *31*, 3680-3682; (b) Elgrishi, N.; Chambers, M. B.; Artero, V.; Fontecave, M. *Phys. Chem. Chem. Phys.* **2014**, *16*, 13635-13644; (c) Bourrez, M.; Molton, F.; Chardon-Noblat, S.; Deronzier, A. *Angew. Chem. Int. Ed.* **2011**, *50*, 9903-9906.
(25) Fischer, F.; Tropsch, H. *Brennst.-Chem.* **1926**, *7*, 97-104.
(26) Kuehnel, M. F.; Wakerley, D. W.; Orchard, K. L.; Reisner, E. *Angew. Chem., Int. Ed.* **2015**, *54*, 9627-9631.
(27) Pavlishchuk, V. V.; Addison, A. W. *Inorg. Chim. Acta* **2000**, *298*, 97-102.
(28) Krejčik, M.; Daněk, M.; Hartl, F. *Journal of Electroanalytical Chemistry and Interfacial Electrochemistry* **1991**, *317*, 179-187.
(29) Wakerley, D. W.; Reisner, E. *Phys. Chem. Chem. Phys.* **2014**, *16*, 5739-5746.
(30) Wang, M.; England, J.; Weyhermüller, T.; Wieghardt, K. *Eur. J. Inorg. Chem.* **2015**, *2015*, 1511-1523.
(31) Sampson, M. D.; Froehlich, J. D.; Smieja, J. M.; Benson, E. E.; Sharp, I. D.; Kubiak, C. P. *Energy Environ. Sci.* **2013**, *6*, 3748-3755.
(32) Chang, C. M.; Orchard, K. L.; Martindale, B. C. M.; Reisner, E. *J. Mater. Chem. A* **2016**, *4*, 2856-2862.
(33) Simon, T.; Bouchonville, N.; Berr, M. J.; Vaneski, A.; Adrović, A.; Volbers, D.; Wyrwich, R.; Döblinger, M.; Susha, A. S.; Rogach, A. L.; Jäckel, F.; Stolarczyk, J. K.; Feldmann, J. *Nat. Mater.* **2014**, *13*, 1013-1018.
(34) Moulder, J. F.; Stickle, W. F.; Sobol, P. E.; Bomben, K. D. *Handbook of X-ray Photoelectron Spectroscopy*; Physical Electronics Inc.: Minnesota, 1992.
(35) Elgrishi, N. *PhD thesis*; Université Pierre et Marie Curie: Paris, 2015.
(36) (a) Wang, J.-J.; Li, Z.-J.; Li, X.-B.; Fan, X.-B.; Meng, Q.-Y.; Yu, S.; Li, C.-B.; Li, J.-X.; Tung, C.-H.; Wu, L.-Z. *ChemSusChem* **2014**, *7*, 1468-1475; (b) Li, Z.-J.; Fan, X.-B.; Li, X.-B.; Li, J.-X.; Ye, C.; Wang, J.-J.; Yu, S.; Li, C.-B.; Gao, Y.-J.; Meng, Q.-Y.; Tung, C.-H.; Wu, L.-Z. *J. Am. Chem. Soc.* **2014**, *136*, 8261-8268; (c) Han, Z.; Qiu, F.; Eisenberg, R.; Holland, P. L.; Krauss, T. D. *Science* **2012**, *338*, 1321-1324.

(37) (a) Nakada, A.; Koike, K.; Maeda, K.; Ishitani, O. *Green Chem.* **2016**, *18*, 139-143; (b) Nakada, A.; Koike, K.; Nakashima, T.; Morimoto, T.; Ishitani, O. *Inorg. Chem.* **2015**, *54*, 1800-1807; (c) Ikuta, N.; Takizawa, S.-y.; Murata, S. *Photochem. Photobiol. Sci.* **2014**, *13*, 691-702.

Table of Contents artwork: